

# EDTA-mediated morphology and tunable optical properties of $\text{Eu}^{3+}$ -doped $\text{NaY}(\text{MoO}_4)_2$ phosphor

Xingxing Yang<sup>1</sup> · Zuoling Fu<sup>1</sup> · Chunpeng Zhang<sup>1</sup> · Zhijian Wu<sup>2</sup> · Tianqi Sheng<sup>1</sup>

Received: 28 March 2015 / Accepted: 25 May 2015 / Published online: 3 June 2015  
© Springer Science+Business Media New York 2015

**Abstract** Uniform and well-crystallized  $\text{NaY}(\text{MoO}_4)_2$ :  $\text{Eu}^{3+}$  3D hierarchical flower-like architectures self-assembled from different building blocks have been successfully synthesized by a facile ethylene diamine tetraacetic acid (EDTA)-mediated hydrothermal route. The crystalline phase, size, morphology, and down-conversion luminescence properties were systematically characterized using powder X-ray diffraction, field emission-scanning electron microscopy, photoluminescence (PL) and photoluminescent excitation spectra (PLE), respectively. It was found that the pH value in the initial solution was responsible for the crystal phase determination of final products. The experimental results showed that the amount of EDTA was a key parameter which not only determined their spacial arrangement, but also affected the down-conversion luminescence intensity of the final products. In PL spectrum, a prominent red emission was observed due to the hypersensitive  $^5\text{D}_0 \rightarrow ^7\text{F}_2$  transition, and the optimum doping level of  $\text{Eu}^{3+}$  was 20 %. Two strongest lines at 396 and 467 nm in excitation spectra of these phosphors matched well with the two popular emissions from near ultraviolet and blue GaN-based LEDs, so they could be explored for an efficient red region for white light-emitting diodes.

## 1 Introduction

Nowadays, red phosphors are being developed as photoluminescence (PL) phosphors for white light-emitting diodes (w-LEDs) [1–5]. W-LEDs, the so-called next generation solid-state lighting (SSL) technology, are the current research focus in the lighting industry, due to their advantages of high efficiency, compactness, long operational lifetime, and environmental friendliness. Generally, W-LEDs can be fabricated by combining GaN-based blue chips with YAG:  $\text{Ce}^{3+}$  yellow phosphors, but lacks a red component, resulting in a low color rendering index ( $R_a < 80$ ) and high color temperature ( $T_c > 7000$  K) [6–8]. Therefore, it is of high interest to search for a stable red-emitting phosphor with a high absorption in the near-ultraviolet or blue spectral region [9, 10].

Recently, trivalent rare earth ions doped micro/nanocrystals materials have played an important role in modern lighting and display fields due to their unique electronic, optical, and chemical properties [11, 12]. The PL emission from rare earth doped materials arises due to the transitions within the  $4f^n$  energy manifolds which are forbidden because of the electric dipole selection rule but these are allowed due to the mixing of configurations having opposite parity. Compared with other available luminescence materials, such as organic fluorescent dyes and semiconductor quantum dots, rare-earth ion-doped materials have low toxicity, photostability, high thermal and chemical stability, high luminescence quantum yield (QY), and sharp emission bands [13]. There has been a growing interest in solid-state materials such as vanadates, tungstates, and molybdates doped with rare earths owing to their long wavelength excitation properties and excellent chemical stabilities [9, 14–17]. These compounds have broad and intense charge transfer absorption bands in the

✉ Zuoling Fu  
zlfu@jlu.edu.cn

<sup>1</sup> State Key Laboratory of Superhard Materials, College of Physics, Jilin University, Changchun 130012, China

<sup>2</sup> State Key Laboratory of Rare Earth Resources Utilization, Changchun Institute of Applied Chemistry, Chinese Academy of Sciences, Changchun 130022, China

near ultraviolet (NUV) range and are, therefore, capable of efficiently capturing emissions over a large range of wavelengths with proper luminescent centers. However, much less is known about the properties of lanthanoids, molybdates, and oxomolybdates, which are ternary oxides of alkaline-earth elements.

Several chemical synthesis techniques to prepare rare earth doped phosphors are available such as sol–gel, coprecipitation, microwave, combustion, hydrothermal [18–20], and all these techniques produce high homogeneity of the ultimate product. But, hydrothermal technique is better over other solution phase conventional techniques in terms of its better homogeneity, low cost, low processing temperature, less energy consumption and uniformity in particle size [21, 22]. Moreover, the luminescent intensity can be enhanced in the uniform microcrystals rather than that of agglomerates of distorted particles [23, 24]. Particularly, during the hydrothermal process, through properly employing organic additives with functional groups to the reaction system, the morphology of the targeted material can be effectively controlled since the additive can selectively adhere to some specific crystallographic facet and effectively slows the growth of that facet relative to others, thus modify the crystal growth dynamically [25, 26].

In the current study, we report an efficient method for the controlled fabrication of novel 3D hierarchical architectures of  $\text{NaY}(\text{MoO}_4)_2$  with a high yield and good uniformity via a facile and mild hydrothermal method in EDTA-mediated processes, which is different from the previous published works [22, 27–29]. The effects of the contents of  $\text{Eu}^{3+}$  and the amount of ethylene diamine tetraacetic acid (EDTA) introduced into the reaction systems on the down-conversion luminescence intensity are discussed in detail. These results indicate that this phosphor material shows great prospect in practical application in various fields of SSL.

## 2 Experimental procedure

### 2.1 Preparation of $\text{NaY}(\text{MoO}_4)_2$ : $\text{Eu}^{3+}$ microcrystals

#### 2.1.1 Materials

All the chemicals were commercially available and used without further purification. Europium oxide (99.99 %) were used as the starting raw materials. All other chemicals used were analytical grade without further purification. The yttrium nitrate hexahydrate ( $\text{Y}(\text{NO}_3)_3 \cdot 6\text{H}_2\text{O}$ ) was used as the yttrium source. Rare earth nitrate ( $\text{Eu}(\text{NO}_3)_3$ ) stock solutions of 0.04 M were prepared by dissolving  $\text{Eu}_2\text{O}_3$  in dilute  $\text{HNO}_3$  under stirring and heating. The ammonium

molybdate tetrahydrate ( $(\text{NH}_4)_6\text{Mo}_7\text{O}_{24} \cdot 4\text{H}_2\text{O}$ ) was used as the molybdenum source and sodium hydroxide (NaOH) as the sodium source. Meanwhile, EDTA was used as the “shape modifier”.

#### 2.1.2 Synthesis of $\text{Eu}^{3+}$ -doped $\text{NaY}(\text{MoO}_4)_2$

In a typical synthesis procedure, stoichiometric amounts of  $\text{Y}(\text{NO}_3)_3 \cdot 6\text{H}_2\text{O}$  and  $\text{Eu}(\text{NO}_3)_3$  was dissolved in 20 mL deionized water. Subsequently, a predetermined amount of EDTA (ranging from 0.3 to 0.55 g) was added to form an  $\text{Y}^{3+}$ –EDTA complex. After vigorous stirring for 10 min, 16 mL aqueous solution containing 0.6286 mmol  $(\text{NH}_4)_6\text{Mo}_7\text{O}_{24} \cdot 4\text{H}_2\text{O}$  was added dropwise into the above solution under continuous strong magnetic stirring at room temperature. The pH of the milky colloidal solution was adjusted to a specific value by adding a desired amount of NaOH solution (7 M). NaOH immediately reacted with the resulting white suspension, and a slurry-like white precipitate was formed. After additional agitation for 1 h, the as-obtained mixing solution was poured into a Teflon bottle held in a stainless steel autoclave, sealed and maintained at 180 °C for 24 h. The systems were then allowed to air-cool to room temperature. The final products were separated by means of centrifugation, washed with ethanol and deionized water in sequence, and finally dried in vacuum at 60 °C for 6 h. Finally, the uniform distribution  $\text{NaY}(\text{MoO}_4)_2$ : 0.04 $\text{Eu}^{3+}$  microflowers were obtained.

## 2.2 Characterization

The powder X-ray diffraction (XRD) measurements were performed on a Rigaku-Dmax 2500 diffractometer at a scanning rate of 15°/min in the 2 $\theta$  range from 10° to 65°, with graphite monochromatized Cu K $\alpha$  radiation ( $\lambda = 0.15405$  nm). The morphology and size of the obtained samples were examined by a field emission-scanning electron microscope (FE-SEM, XL30, Philips). The ultraviolet–visible PL excitation and emission spectra were recorded using a Hitachi F-7000 spectrophotometer equipped with a Xe-lamp as an excitation source. All the measurements were performed at room temperature.

## 3 Results and discussion

### 3.1 Crystal structure and morphology of the $\text{NaY}(\text{MoO}_4)_2$ : $\text{Eu}^{3+}$ microflowers

#### 3.1.1 XRD

The composition and phase purity of the as-synthesized products were characterized by XRD. Figure 1 showed the

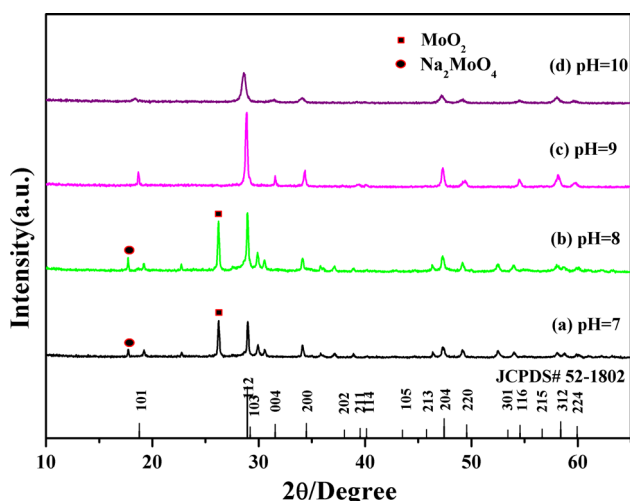


**Fig. 1** XRD powder patterns of  $\text{NaY}(\text{MoO}_4)_2$  samples prepared by hydrothermal method at 180 °C for 24 h with the assistance of 0.45 g EDTA at (a) pH = 7; (b) pH = 8; (c) pH = 9; (d) pH = 10. The standard data for  $\text{NaY}(\text{MoO}_4)_2$  (JCPDS card 52-1802) are also presented for comparison

representative XRD diffractogram of the hydrothermal reaction products prepared at different pH values for 24 h at 180 °C in the presence of 0.45 g EDTA. Different pH values for the synthesis of single phase crystalline  $\text{NaY}(\text{MoO}_4)_2: \text{Eu}^{3+}$  powders were investigated by varying the base (NaOH) concentration used in the reaction process. When the value of  $\text{pH} \leq 8$  (Fig. 1a pH = 7 and 1b pH = 8), some of  $\text{MoO}_2$  and  $\text{Na}_2\text{MoO}_4$  impurity peaks were detected in the XRD patterns, whereas beginning with pH = 9 (Fig. 1c), no impurity lines were discovered in this experimental range, all diffraction peaks of the sample could be consistent with the pure tetragonal phase of  $\text{NaY}(\text{MoO}_4)_2$  (JCPDS #52-1802) with  $I4_1/a$  lattice symmetry. Furthermore, the crystallization had reached completion with strong and sharp diffraction peaks at the pH value of 9, showing that the  $\text{Eu}^{3+}$  ions were entirely incorporated in the  $\text{NaY}(\text{MoO}_4)_2$  host lattice at the present doping level by substituting for the  $\text{Y}^{3+}$ . In addition, when the value of pH = 10, we also could acquire the pure phase (Fig. 1d). From the analysis above, we could conclude that the pH value was undoubtedly vital in preparing the pure phase  $\text{NaY}(\text{MoO}_4)_2$  in the current study.

The typical powder XRD patterns of the as-obtained  $\text{NaY}(\text{MoO}_4)_2$  products acquired with the assistance of different amounts of EDTA at pH = 9 were presented in Fig. 2. Compared with the standard card of tetragonal  $\text{NaY}(\text{MoO}_4)_2$ , all diffraction peaks of the different samples could be well indexed to pure phase. Furthermore, it could be observed that the intensity of the diffraction lines increased and reached a maximum at 0.45 g of EDTA with increasing the amount of EDTA. When the amount of

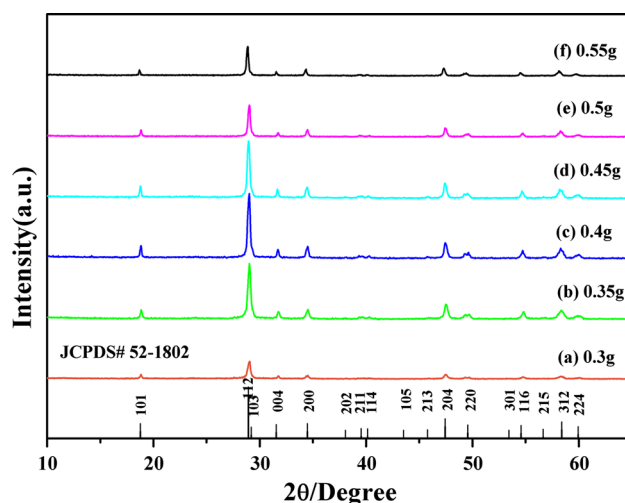


**Fig. 2** XRD patterns of the as-synthesized products obtained at pH = 9 in the presence of different amounts of EDTA. (a) 0.30 g EDTA; (b) 0.35 g EDTA; (c) 0.40 g EDTA; (d) 0.45 g EDTA; (e) 0.50 g EDTA; (f) 0.55 g EDTA. The standard data for  $\text{NaY}(\text{MoO}_4)_2$  (JCPDS card no. 52-1802) was shown as reference

EDTA was more than 0.45 g, the intensity of the diffraction lines tended to decrease. No other impurity peaks were observed, revealing the high purity of the as-prepared samples. In the latter work, it was also found that the amount of EDTA introduced to the reaction system had a crucial effect on the morphology and down-conversion luminescence properties of the  $\text{Eu}^{3+}$  ions doped phosphors.

### 3.1.2 FE-SEM

In the synthesis of inorganic nano/microcrystals many organic additives have been employed for the modifications of certain crystallographic surfaces [30–33]. As is well known, EDTA possesses four carboxyl groups ( $-\text{COOH}$ ) and two lone pairs of electrons on two nitrogen atoms which can act as binding sites. These characters endow EDTA with a strong chelating ability and an excellent capping ability, which can effectively modulate the growth rates of different facets. In this work, when EDTA is added into  $\text{Y}(\text{NO}_3)_3$  solution, it can coordinate with  $\text{Y}^{3+}$  ions to form the intermediate complex of  $\text{Y}^{3+}\text{-EDTA}$ , which greatly decreases the concentration of free  $\text{Y}^{3+}$  in solution and helps to control the nucleation and growth of high-quality crystals in view of the dynamic process. Then, the introduction of molybdate into  $\text{Y}^{3+}\text{-EDTA}$  leads to the competition of  $\text{MoO}_4^{2-}$  for  $\text{Y}^{3+}$  with EDTA and the formation of  $\text{NaY}(\text{MoO}_4)_2$  nanoparticles. From the thermodynamic viewpoint, the incipient nanoparticles have a tendency to self-aggregate into larger particles to minimize the surface energy [34]. The morphology of the as-prepared  $\text{NaY}(\text{MoO}_4)_2: \text{Eu}^{3+}$  hierarchical flower-like architectures

was first examined by field emission-scanning electron microscopy (FE-SEM). Figure 3 illustrated the representative FE-SEM images of the samples prepared hydrothermally at 180 °C for 24 h at pH = 9. The panoramic FE-SEM images were shown the range of morphologies achievable through the current approach, depending on the amount of EDTA (from 0.30 to 0.55 g) under otherwise

identical reaction conditions. We viewed the gradual morphology evolution of resultant  $\text{NaY}(\text{MoO}_4)_2 \cdot \text{Eu}^{3+}$  crystallites as the amount of EDTA was increased. As shown in Fig. 3a, the product formed in the presence of 0.30 g EDTA was almost entirely composed of tiny irregular microsheets containing nanoparticles without a discernable morphology. When 0.35 g of EDTA was added, we obtained self-

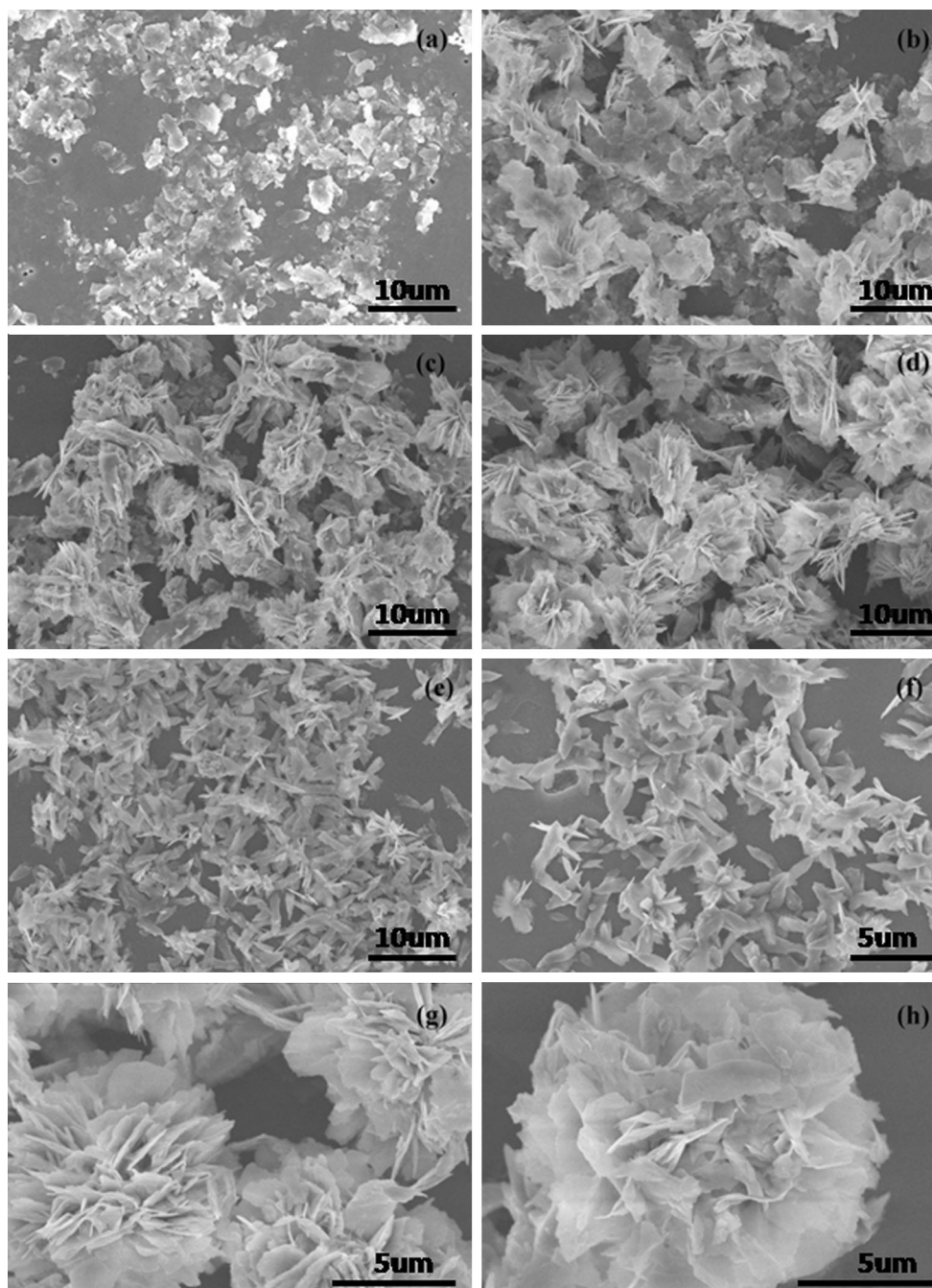


**Fig. 3** FE-SEM images of  $\text{NaY}(\text{MoO}_4)_2 \cdot \text{Eu}^{3+}$  crystallites prepared hydrothermally at 180 °C for 24 h at pH = 9 with the assistance of different amounts of EDTA. **a** 0.30 g EDTA; **b** 0.35 g EDTA;

**c** 0.40 g EDTA; **d** 0.45 g EDTA; **e** 0.50 g EDTA; **f** 0.55 g EDTA; **g** magnified images of the flower-like microstructures (0.45 g EDTA); **h** detailed view of an individual microflower (0.45 g EDTA)

assembled microflowers with intercrossing petals, including many nano-fragments (Fig. 3b). With the further increment of the EDTA amount (0.40 g), more and more nanoplates aggregated together to form flower-like polymerides (Fig. 3c). When the amount of EDTA was 0.45 g (Fig. 3d), well dispersed uniform  $\text{NaY}(\text{MoO}_4)_2$  submicrocrystals with an average diameter of about 10  $\mu\text{m}$  were obtained. As the amount of EDTA was increased to 0.50 and 0.55 g (Fig. 3e, f), the product exhibited some accumulated bulk microcrystals, which were made up of some small plate crystals, and regular microflowers disappeared. In order to investigate the morphology and microstructure of the flower-shaped  $\text{NaY}(\text{MoO}_4)_2$  sample, enlarged FE-SEM images of the microcrystalline were employed in Fig. 3g, h. Higher-magnification FE-SEM images revealed that the 3D hierarchical flower-like architectures were constructed from a great many amorphous tightly interleaved nanoplates. The above-stated results indicated that the introduction of an appropriate amount of EDTA was undoubtedly prerequisite for the formation of such microcrystal textures in the present system since the additive could selectively adhere to some specific crystallographic facet and thus modified the crystal growth dynamically [35–38].

### 3.2 Down-conversion photoluminescence of $\text{NaY}(\text{MoO}_4)_2: \text{Eu}^{3+}$ microflowers

$\text{NaY}(\text{MoO}_4)_2$ , which shares scheelite-like structures, shows excellent thermal and hydrolytic stability and is demonstrated to be an efficient host for other lanthanide ions to produce various luminescence properties [22, 27, 39–42]. The  $\text{Eu}^{3+}$  ion is a well-known red-emitting activator in commercial phosphors because the emission of the rare-earth  $\text{Eu}^{3+}$  ion consists usually of lines in the red spectral area due to the  $^5\text{D}_0 \rightarrow ^7\text{F}_J$  ( $J = 1, 2, 3, 4, 5$  and  $6$ ) transitions, so it is of technological importance for improving their PL properties. It is noteworthy that doping with  $\text{Eu}^{3+}$  alters neither the crystal structure nor the morphology of the host material due to the similarity of  $\text{Eu}^{3+}$  to  $\text{Y}^{3+}$ .

At the same level of  $\text{Eu}^{3+}$ , the  $\text{NaY}(\text{MoO}_4)_2: \text{Eu}^{3+}$  phosphors are prepared hydrothermally at 180 °C for 24 h at pH = 9 with the assistance of different amounts of EDTA and the evolution of the excitation and emission spectra as the increasing of the EDTA amount at room temperature are depicted in Figs. 4 and 5, respectively. All spectra are similar in the shapes and locations excluding relative intensities, the difference in fluorescence intensity of them can be ascribed to the combined roles of their various dimensions, morphology, and the degree of crystallinity. With the change of the EDTA amount from 0.3 to 0.55 g, the excitation and emission intensities increase gradually and reach maximum at 0.45 g, which are consistent with the results of XRD and FE-SEM. The

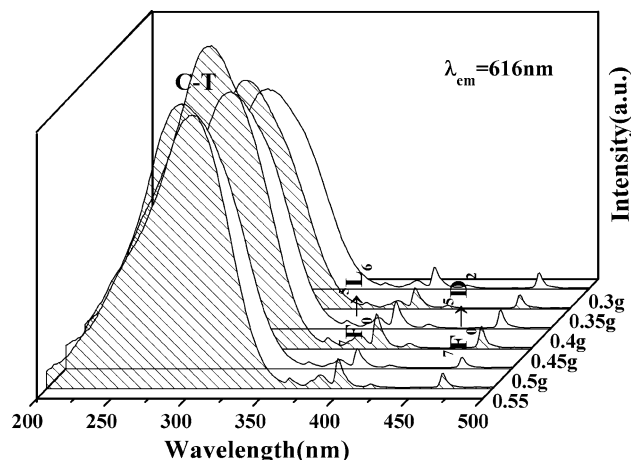


**Fig. 4** Room-temperature PL excitation spectra ( $\lambda_{\text{em}} = 616 \text{ nm}$ ) of  $\text{NaY}(\text{MoO}_4)_2: \text{Eu}^{3+}$  microcrystals with different amounts of EDTA

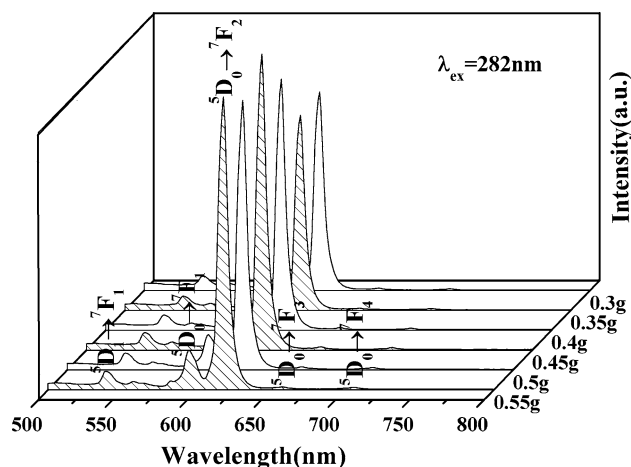
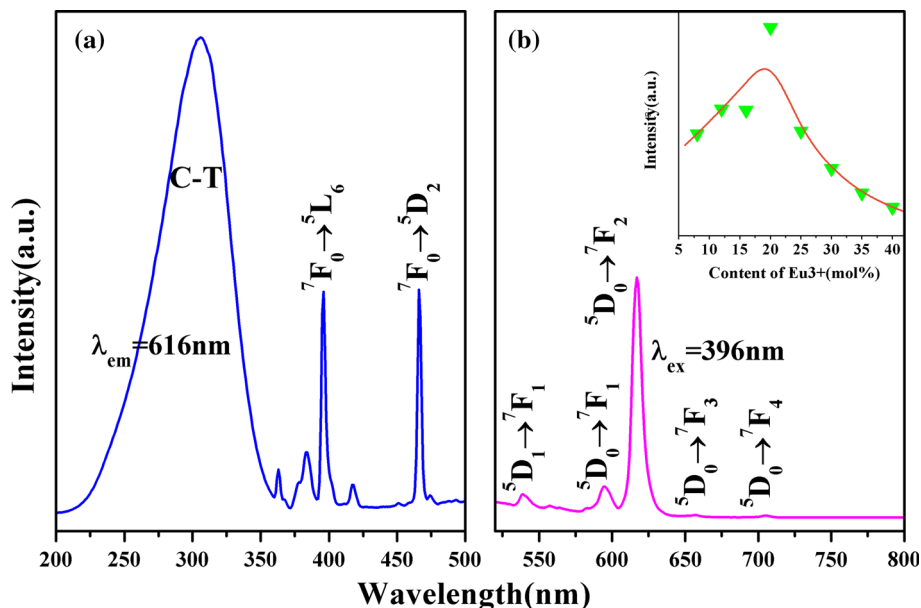


**Fig. 5** Room-temperature PL emission spectra ( $\lambda_{\text{ex}} = 282 \text{ nm}$ ) of  $\text{NaY}(\text{MoO}_4)_2: \text{Eu}^{3+}$  microcrystals with different amounts of EDTA

morphology and PL are optimal when the amount of EDTA is 0.45 g. The excitation spectra (Fig. 4) are obtained by monitoring the emission of the  $\text{Eu}^{3+} ^5\text{D}_0 \rightarrow ^7\text{F}_2$  transition at 616 nm. It can be observed clearly that the excitation spectrum contains a strong broad band between 200 and 360 nm centered around 282 nm, which corresponds to the O–Mo charge transfer transition [ligand to metal charge transfer (LMCT)] [43, 44]. In addition, there are some excitation peaks in the longer wavelength range of 360–500 nm and the sharp lines at 396 ( $^7\text{F}_0 \rightarrow ^5\text{L}_6$ ) and 467 nm ( $^7\text{F}_0 \rightarrow ^5\text{D}_2$ ) are associated with the typical intra-4f transitions of  $\text{Eu}^{3+}$  ion. Upon excitation into the  $\text{MoO}_4^{2-}$  at 282 nm (Fig. 5), the characteristic emission spectrum exhibits five groups of emission lines at 540, 594, 616, 658 and 705 nm correspond to  $^5\text{D}_1 \rightarrow ^7\text{F}_1$  and  $^5\text{D}_0 \rightarrow ^7\text{F}_J$  ( $J = 1, 2, 3, 4$ ) transitions in  $\text{Eu}^{3+}$ , respectively. It is well-known that the intensity ratio of  $^5\text{D}_0 \rightarrow ^7\text{F}_2$  to  $^5\text{D}_0 \rightarrow ^7\text{F}_1$

**Fig. 6** **a** PLE ( $\lambda_{em} = 616$  nm) and **b** PL ( $\lambda_{ex} = 396$  nm) spectra of  $\text{NaY}_{0.80}(\text{MoO}_4)_2: 0.20\text{Eu}^{3+}$  samples prepared hydrothermally at  $\text{pH} = 9$  with the assistance of 0.45 g EDTA. Inset is the dependence of the PL intensities on the contents of  $\text{Eu}^{3+}(x)$



is strongly dependent on the local environment symmetry of the  $\text{Eu}^{3+}$  activators. Therefore,  $\text{Eu}^{3+}$  ions are often used as probes to detect local environment in a matrix. According to Judd–Ofelt theory, when  $\text{Eu}^{3+}$  ions are located in a site with inversion symmetry, the  ${}^5\text{D}_0\text{--}{}^7\text{F}_1$  magnetic dipole transition will dominate; on the contrary, when a  $\text{Eu}^{3+}$  ion site is noncentrosymmetric, the  ${}^5\text{D}_0\text{--}{}^7\text{F}_2$  electric dipole transitions will be preponderant in the emission [45]. In this case,  $\text{NaY}(\text{MoO}_4)_2: \text{Eu}^{3+}$  has a tetragonal scheelite structure with space group  $I4_1/a$ , in which  $\text{Y}^{3+}$  is coordinated with eight oxygen atoms and has a  $S_4$  point symmetry with no inversion center. The emission spectra are dominated by the red  ${}^5\text{D}_0\text{--}{}^7\text{F}_2$  transition of  $\text{Eu}^{3+}$  at 616 nm, which is an electric-dipole-allowed transition and indicates that the  $\text{Eu}^{3+}$  ions occupy a center of asymmetry in the crystal lattice. Although no emission corresponding to  $\text{MoO}_4^{2-}$  groups is observed, the presence of an absorption band originating from the  $\text{MoO}_4^{2-}$  groups is detected in the excitation spectrum when monitoring at 616 nm. This fact suggests that the energy absorbed by the  $\text{MoO}_4^{2-}$  group is transferred to  $\text{Eu}^{3+}$  ion levels nonradiatively. So the emission corresponding to  $\text{Eu}^{3+}$  ions has been observed under excitation of the CT band of the  $\text{MoO}_4^{2-}$  group, and this process has been known as host-sensitized energy transfer [46]. In addition, we have studied the effect of dopant concentration of  $\text{Eu}^{3+}$  ions. Inset of Fig. 6b depicts the dependence of the PL emission intensity (the integrated area under the PL profile from 604 to 646 nm) upon the  $\text{Eu}^{3+}$  concentration with 396 nm NUV light irradiation. With the concentration of  $\text{Eu}^{3+}$  ion varying from low to high, the intensity of emission is enhanced linearly until the

doping level of 20 % followed by a remarkable decline due to the concentration quenching effect. Room-temperature PL excitation spectrum ( $\lambda_{em} = 616$  nm) and PL emission spectrum ( $\lambda_{ex} = 396$  nm) of  $\text{NaY}_{0.80}(\text{MoO}_4)_2: 0.20 \text{Eu}^{3+}$  (the optimal doping concentration) phosphors synthesized by hydrothermal method at 180 °C for 24 h at  $\text{pH} = 9$  with the assistance of 0.45 g EDTA are displayed in Fig. 6a, b. It can be visually observed from Fig. 6a that the samples have an effective and intrinsic absorption at about 396 and 467 nm associated with the typical intra-4f transitions of  $\text{Eu}^{3+}$  ion, which makes them match well with the near-UV and blue GaN-based LED chips, respectively. To summarize, the  $\text{NaY}(\text{MoO}_4)_2: \text{Eu}^{3+}$  flower-like architectures synthesized in our experiment are a kind of efficient phosphor with high color purity and strong red luminescence, and may be applied as a red component for white light emitting diodes (W-LEDs).

#### 4 Conclusion

In conclusion, the  $\text{NaY}(\text{MoO}_4)_2$  microcrystals doped with  $\text{Eu}^{3+}$  ions have been successfully prepared by a hydrothermal method in an EDTA-mediated processes. The results indicate that the amount of EDTA and pH value of the precursor solution are found to be crucial in determining the crystal phase. The gradual morphology evolution and the evolution of down-conversion fluorescent intensity of  $\text{NaY}(\text{MoO}_4)_2: \text{Eu}^{3+}$  as the increasing of the EDTA amount have been investigated in detail. A crystallization pH value of 9 and EDTA amount of 0.45 g are optimal for the pure-phase synthesis, the uniform morphology and the luminescence intensity of  $\text{NaY}(\text{MoO}_4)_2$

microcrystalline. The PL properties of  $\text{Eu}^{3+}$  ion activated  $\text{NaY}(\text{MoO}_4)_2$  are investigated. We can observe the concentration quenching of  $\text{Eu}^{3+}$  emission when the  $\text{Eu}^{3+}$  doping level exceed 20 mol%. The as-obtained hierarchical  $\text{NaY}(\text{MoO}_4)_2: \text{Eu}^{3+}$  microflowers exhibit intense red emission, so the samples may have potential applications in the red components for light display systems as well as optoelectronic devices.

**Acknowledgments** This work was supported by the Science and Technology Development Planning Project of Jilin Province (20130522173JH), partially sponsored by China Postdoctoral Science Foundation, supported by National Found for Fostering Talents of Basic Science (No. J1103202) and by Outstanding Young Teacher Cultivation Plan in Jilin University.

## References

- R.J. Xie, N. Hirosaki, Silicon-based oxynitride and nitride phosphors for white LEDs: a review. *Sci. Technol. Adv. Mater.* **8**, 588–600 (2007)
- L.C. Ju, C. Cai, Q.Q. Zhu, J.Y. Tang, L.Y. Hao, X. Xu, Color tunable  $\text{Sr}_2\text{SiO}_4: \text{Eu}^{2+}$  phosphors through the modification of crystal structure. *J. Mater. Sci. Mater. Electron.* **24**, 4516–4521 (2013)
- Z.G. Xia, Y.J. Liang, W.Z. Huang, M.F. Zhang, D.Y. Yu, J.M. Wu, J.W. Zhao, M.H. Tong, Q. Wang, Molten salt synthesis and photoluminescence properties of novel red emitting phosphors  $\text{Ba}_5(\text{VO}_4)_3\text{Cl}: \text{Eu}^{3+}, \text{K}^{3+}$ . *J. Mater. Sci. Mater. Electron.* **24**, 5111–5116 (2013)
- P. Li, Z. Wang, Z. Yang, Q. Guo,  $\text{Sr}_2\text{B}_2\text{P}_2\text{O}_{10}: \text{Eu}^{2+}, \text{Mn}^{2+}, \text{Ba}^{2+}$ : a potential single-phase white light-emitting phosphor for UV light emitting diode. *J. Electrochem. Soc.* **157**, H504–H509 (2010)
- Z.W. Zhang, L. Liu, Y.H. Wang, S.T. Song, D.J. Wang, Preparation and luminescence properties of  $\text{Sr}_7\text{Zr}(\text{PO}_4)_6: \text{Dy}^{3+}$  single-phase full-color phosphor. *J. Mater. Sci. Mater. Electron.* **26**, 4202–4206 (2015)
- A. Setlur, W.J. Heward, Y. Gao, A.M. Srivastava, R.G. Chandran, M.V. Shankar, Crystal chemistry and luminescence of  $\text{Ce}^{3+}$ -doped  $\text{Lu}_2\text{CaMg}_2(\text{Si}, \text{Ge})_3\text{O}_{12}$ , and its use in LED based lighting. *Chem. Mater.* **18**, 3314–3322 (2006)
- W.R. Liu, C.H. Huang, C.W. Yeh, J.C. Tsai, Y.C. Chiu, Y.T. Yeh, R.S. Liu, A study on the luminescence and energy transfer of single-phase and color-tunable  $\text{KCaY}(\text{PO}_4)_2: \text{Eu}^{2+}, \text{Mn}^{2+}$  phosphor for application in white-light LEDs. *Inorg. Chem.* **51**, 9636–9641 (2012)
- J.S. Kim, P.E. Jeon, J.C. Choi, H.L. Park, S.I. Mho, G.C. Kim, Warm-white-light emitting diode utilizing a single-phase full-color  $\text{Ba}_3\text{MgSi}_2\text{O}_8: \text{Eu}^{2+}, \text{Mn}^{2+}$  phosphor. *Appl. Phys. Lett.* **84**, 2931–2934 (2004)
- S. Neeraj, N. Kijima, A.K. Cheetham, Novel red phosphors for solid-state lighting: the system  $\text{NaM}(\text{WO}_4)_{2-x}(\text{MoO}_4)_x: \text{Eu}^{3+}$  ( $\text{M} = \text{Gd}, \text{Y}, \text{Bi}$ ). *Chem. Phys. Lett.* **387**, 2–6 (2004)
- K.Y. Jung, J.H. Kim, Y.C. Kang, Luminescence enhancement of eu-doped calcium magnesium silicate blue phosphor for UV-LED application. *J. Lumin.* **129**, 615–619 (2009)
- F. Wang, Y. Han, C.S. Lim, Y.H. Lu, J. Wang, J. Xu, H.Y. Chen, C. Zhang, M.H. Hong, X.G. Liu, Simultaneous phase and size control of upconversion nanocrystals through lanthanide doping. *Nature* **463**, 1061–1065 (2010)
- K. Riwozki, H. Meyssamy, H. Schnablegger, A. Kornowski, M. Haase, Liquid-phase synthesis of colloids and redispersible powders of strongly luminescing  $\text{LaPO}_4: \text{Ce}, \text{Tb}$  nanocrystals. *Angew. Chem. Int. Ed.* **40**, 573–576 (2001)
- Y. Lu, H.Z. Yu, Influence of the  $\text{Eu}^{3+}$  dosage concentration on luminescence properties of  $\text{YPO}_4: \text{Eu}^{3+}$  microspheres. *J. Mater. Sci. Mater. Electron.* **25**, 1013–1016 (2014)
- A. Huignard, T. Gaoïn, J.P. Boilot, Synthesis and luminescence properties of colloidal  $\text{YVO}_4: \text{Eu}$  phosphors. *Chem. Mater.* **12**, 1090–1094 (2000)
- S. Neeraj, N. Kijima, A.K. Cheetham, Novel red phosphors for solid state lighting; the system  $\text{Bi}_x\text{Ln}_{1-x}\text{VO}_4: \text{Eu}^{3+}/\text{Sm}^{3+}$  ( $\text{Ln} = \text{Y}, \text{Gd}$ ). *Solid State Commun.* **131**, 65–69 (2004)
- L. Macalik, M. Maczka, J. Hanuza, A. Hanuza, Structure and properties of the  $\text{KNbW}_2\text{O}_9$  hexagonal bronze doped with  $\text{Eu}^{3+}$  ions as an optically active probe. *J. Alloys Compd.* **380**, 248–254 (2004)
- V.F. Zolin, S.N. Vetkina, V.M. Markushev, Oxotungstates of lanthanum and alkaline-earth elements as materials for neodymium powder lasers. *Sov. J. Quantum Electron.* **18**, 204–206 (1988)
- J.H. Zhang, W. Lv, Z.D. Hao, Color-tunable white-light emitting  $\text{BaMg}_2\text{Al}_6\text{Si}_9\text{O}_{30}: \text{Eu}^{2+}, \text{Tb}^{3+}, \text{Mn}^{2+}$  phosphors via energy transfer. *Chin. Opt.* **5**(3), 203–208 (2012). (in Chinese)
- H.Y. Du, Z.P. Wei, L.J. Sun, Luminescent properties of  $\text{ZnS}: \text{Mn}$  nanoparticles dependent on doping concentration. *Chin. Opt.* **6**(1), 111–116 (2013). (in Chinese)
- F. Wang, X.P. Fan, D.B. Pi, Hydrothermal synthesis and luminescence behavior of rare-earth-doped  $\text{NaLa}(\text{WO}_4)_2$  powders. *J. Solid State Chem.* **178**(3), 825–830 (2005)
- J.S. Liao, B. Qiu, H.S. Lai, Synthesis and luminescence properties of  $\text{Tb}^{3+}: \text{NaGd}(\text{WO}_4)_2$  novel green phosphors. *J. Lumin.* **129**, 668–671 (2009)
- Y. Li, G.F. Wang, K. Pan, Y. Qu, S. Liu, L. Feng, Formation and down/up conversion luminescence of  $\text{Ln}^{3+}$  doped  $\text{NaY}(\text{MoO}_4)_2$  microcrystals. *Dalton Trans.* **42**, 3366–3372 (2013)
- N. Banerjee, S.B. Krupanidhi, Facile hydrothermal synthesis and observation of bubbled growth mechanism in nano-ribbons aggregated microspherical Covellite blue-phosphor. *Dalton Trans.* **39**, 9789–9793 (2010)
- J. Wang, Y.H. Xu, M. Hojamberdiev, Hydrothermal synthesis of well-dispersed  $\text{YVO}_4: \text{Eu}^{3+}$  microspheres and their photoluminescence properties. *J. Alloy. Compd.* **481**, 896–902 (2009)
- R.Q. Song, A.W. Xu, S.H. Yu, Layered copper metagermanate nanobelts: hydrothermal synthesis, structure, and magnetic properties. *J. Am. Chem. Soc.* **129**, 4152–4153 (2007)
- Y.D. Yin, A.P. Alivisatos, Colloidal nanocrystal synthesis and the organic–inorganic interface. *Nature* **437**, 664–670 (2005)
- Z.H. Xu, C.X. Li, G.G. Li, R.T. Chai, C. Peng, D.M. Yang, J. Lin, Self-assembled 3D urchin-like  $\text{NaY}(\text{MoO}_4)_2: \text{Eu}^{3+}/\text{Tb}^{3+}$  microarchitectures: hydrothermal synthesis and tunable emission colors. *J. Phys. Chem. C* **114**, 2573–2582 (2010)
- Y. Huang, L.Q. Zhou, L. Yang, Z.W. Tang, Self-assembled 3D flower-like  $\text{NaY}(\text{MoO}_4)_2: \text{Eu}^{3+}$  microarchitectures: hydrothermal synthesis, formation mechanism and luminescence properties. *Opt. Mater.* **33**, 777–782 (2011)
- Y.J. Zhang, W. Zhu, H.M. He, A. Zheng, Synthesis of flower-like  $\text{NaY}(\text{MoO}_4)_2$  and optical property of  $\text{NaY}(\text{MoO}_4)_2: \text{Eu}^{3+}$ . *Chin. J. Chem. Phys.* **26**, 451–456 (2013)
- F. Li, Y. Ding, P.X. Cao, X.Q. Xin, Z.L. Wang, Single-Crystal hexagonal disks and rings of  $\text{ZnO}$ : low-temperature, large-scale synthesis and growth mechanism. *Angew. Chem.* **43**, 5238–5242 (2004)
- C.L. Kuo, T.J. Kuo, M.H. Huang, Hydrothermal synthesis of  $\text{ZnO}$  microspheres and hexagonal microrods with sheetlike and

- platelike nanostructures. *J. Phys. Chem. B* **109**, 20115–20121 (2005)
32. W.D. Shi, L.H. Huo, H.S. Wang, H.J. Zhang, J.H. Yang, P.H. Wei, Hydrothermal growth and gas sensing property of flower-shaped SnS<sub>2</sub> nanostructures. *Nanotechnology* **17**, 2918–2924 (2006)
33. N.R. Jana, L.A. Gearheart, S.O. Obare, C.J. Johnson, K.J. Edler, S. Mann, C.J. Murphy, Liquid crystalline assemblies of ordered gold nanorods. *J. Mater. Chem.* **12**, 2909–2912 (2002)
34. Y. Chang, J.J. Teo, H.C. Zeng, Formation of colloidal CuO nanocrystallites and their spherical aggregation and reductive transformation to hollow Cu<sub>2</sub>O nanosphere. *Langmuir* **21**, 1074–1079 (2005)
35. V.F. Puentes, D. Zanchet, C.K. Erdonmez, A.P. Alivisatos, Synthesis of Hcp-Co nanodisks. *J. Am. Chem. Soc.* **124**, 12874–12880 (2002)
36. W. Wang, J. Zhuang, Q. Peng, Y.D. Li, Liquid–solid-solution synthesis of biomedical hydroxyapatite nanorods. *Adv. Mater.* **18**, 2031–2034 (2006)
37. L.W. Qian, J. Zhu, Z. Chen, Y.C. Gui, Q. Gong, Y.P. Yuan, J.T. Zai, X.F. Qian, Self-assembled heavy lanthanide orthovanadate architecture with controlled dimensionality and morphology. *Chem. Eur. J.* **15**, 1233–1240 (2009)
38. C.X. Li, J. Yang, Z.W. Quan, P.P. Yang, D.Y. Kong, J. Lin, Different microstructures of β-NaYF<sub>4</sub> fabricated by hydrothermal process: effects of pH values and fluoride sources. *Chem. Mater.* **19**, 4933–4942 (2007)
39. S.S. Liu, D.P. Yang, D.K. Ma, S. Wang, T.D. Tang, S.M. Huang, Single-crystal NaY(MoO<sub>4</sub>)<sub>2</sub> thin plates with dominant 001 facets for efficient photocatalytic degradation of dyes under visible light irradiation. *Chem. Commun.* **47**, 8013–9015 (2011)
40. J. Liu, B. Xu, C. Song, H.D. Luo, X. Zou, L.X. Han, X.B. Yu, Shape-controlled synthesis of monodispersed nano-/micro-NaY(MoO<sub>4</sub>)<sub>2</sub> (doped with Eu<sup>3+</sup>) without capping agents via a hydrothermal process. *CrystEngComm* **14**, 2936–2943 (2012)
41. Y. Li, G.F. Wang, K. Pan, W. Zhou, C. Wang, N.Y. Fan, Y.J. Chen, Q.M. Feng, B.B. Zhao, Controlled synthesis and luminescence properties of rhombic NaLn(MoO<sub>4</sub>)<sub>2</sub> submicrocrystals. *CrystEngComm* **14**, 5015–5020 (2012)
42. Y.S. Hu, W.D. Zhuang, H.Q. Ye, D.H. Wang, S.S. Zhang, X.W. Huang, A novel red phosphor for white light emitting diodes. *J. Alloys Compd.* **390**, 226–229 (2005)
43. J.A. Groenink, C. Hakfoort, G. Blasse, The luminescence of calcium molybdate. *Phys. Status Solidi A* **54**, 329–336 (1979)
44. T. Yamase, P. Prokop, Y. Arai, Photochemical studies of alkylammonium molybdates. Part 12. O → Mo charge-transfer triplet-states-initiated self-assembly to Mo<sub>154</sub> ring- and tube-molybdenum-blues. *J. Mol. Struct.* **656**, 107–117 (2003)
45. L. Xu, X.Y. Yang, Z. Zhai, X. Chao, Z.H. Zhang, W.H. Hou, EDTA-mediated hydrothermal synthesis of NaEu(MoO<sub>4</sub>)<sub>2</sub> microrugbies with tunable size and enhanced luminescence properties. *CrystEngComm* **13**, 4921–4929 (2011)
46. V. Sivakumar, U.V. Varadaraju, Intense red phosphor for white LEDs based on blue GaN LEDs. *J. Electrochem. Soc.* **153**, H54–H57 (2006)